



Chloride attack on the passive film of duplex alloy

B. Zhang^{a,1,*}, X.X. Wei^{a,b,1}, B. Wu^a, J. Wang^a, X.H. Shao^a, L.X. Yang^a, S.J. Zheng^a, Y.T. Zhou^a, Q.Q. Jin^a, E.E. Oguzie^c, X.L. Ma^{a,d,*}

^a Shenyang National Laboratory for Materials Science (SYNL), Institute of Metal Research, Chinese Academy of Sciences, Wenhua Road 72, 110016, Shenyang, China

^b School of Materials Science and Engineering, University of Science and Technology of China

^c Electrochemistry and Materials Science Research Laboratory, Department of Chemistry, Federal University of Technology Owerri, PMB 1526 Owerri, Nigeria

^d State Key Lab of Advanced Processing and Recycling on Non-ferrous Metals, Lanzhou University of Technology, Lanzhou 730050, China



ARTICLE INFO

Keywords:

Duplex alloy
Passive film
Chloride attack
Cs-corrected TEM

ABSTRACT

Passive films on duplex stainless steels are heterogeneous, with properties depending on the two-phase microstructure. Accordingly, the interaction of chloride ions with the passive films on either of the two phases ought to vary. These issues have been investigated by some indirect methods, not sufficiently nor directly corroborated by experimental evidence. Using aberration-corrected transmission electron microscopy, we simultaneously investigate the films on the ferrite and austenite phase near the phase boundary, as well as the film evolution in chloride-containing media. This study provides some virtual experimental insights into the features of chloride attack on the passive film of duplex alloys.

1. Introduction

Duplex stainless steels (DSSs) are highly important engineering materials, due to their generally high corrosion resistance combined with high strength and moderate cost. The superior corrosion resistance is attributable to the nanometer-thick passive films on these alloys. The nature of the passive film strongly depends on the chemistry of the underlying matrix. Duplex stainless steels have a two-phase microstructure consisting of ferrite and austenite [1]. The four essential alloying elements (Cr, Mo, Ni and N) are not uniformly distributed between the two phases, with Cr and Mo partitioned to the ferrite phase, and Ni and N to the austenite phase [1–5]. As a result, the nature of the passive films on these two phases is expected to be different. Actually, this issue has been extensively studied by means of Auger electron spectroscopy (AES) [1,3,6–8], X-ray photoelectron spectroscopy (XPS) [3,9–11] and second ion mass spectroscopy (SIMS) [8], and the general consensus is that the passive films on these two phases have varied chemical compositions and/or thicknesses.

The equilibrium thickness actually is closely related to the growth dynamics of the passive film and highly dependent on the diffusion of the reactive species in the oxide film [12], alongside the movement of the film/matrix (f/m) interface. Any differences in thickness strongly imply differences in the corresponding growth dynamics of the passive film, and for duplex stainless steels would result in a distinctive region

at the ferrite/austenite interface, different from the bulk of either phase. Precisely, the passive film on DSS has a heterogeneous nature, consisting of the passive films on the austenite and ferrite as well as on the boundary region. Therefore, precise characterization of the composition and structure of the extremely thin passive film near the austenite/ferrite boundary is key to deciphering the nature of the passive film on DSS. Evidently, techniques based strictly on indirect spectroscopy may be insufficient to guarantee precision and accuracy of the obtained information. Furthermore, it is worthwhile to note that in most of the previous studies, the DSS specimens were usually chemical or electrochemically etched in order to make the two phases distinguishable [7,8,13–15]. Such etching pretreatment could inevitably alter the composition of the phase boundary zone, such that any observations or deductions on the nature of the passive film may be far removed from the real situation.

The interaction of chloride ions with the passive films on the two phases of the DSS should as well be different. Indeed, Vignal et al. [8] reported that detection of chloride ions in the passive films on both the ferrite and austenite phases after long-term aging in chloride-containing solutions, with chloride preferentially absorbed in the austenite passive film. There is however no doubt that more precise and accurate assessment of the nature of interactions between the passive film of DSS and chloride ions requires determination of chloride ion distribution in the passive films on the two phases, as well as the evolution of the

* Corresponding authors.

E-mail addresses: bozhang@imr.ac.cn (B. Zhang), xlma@imr.ac.cn (X.L. Ma).

¹ These authors contributed equally to this work.

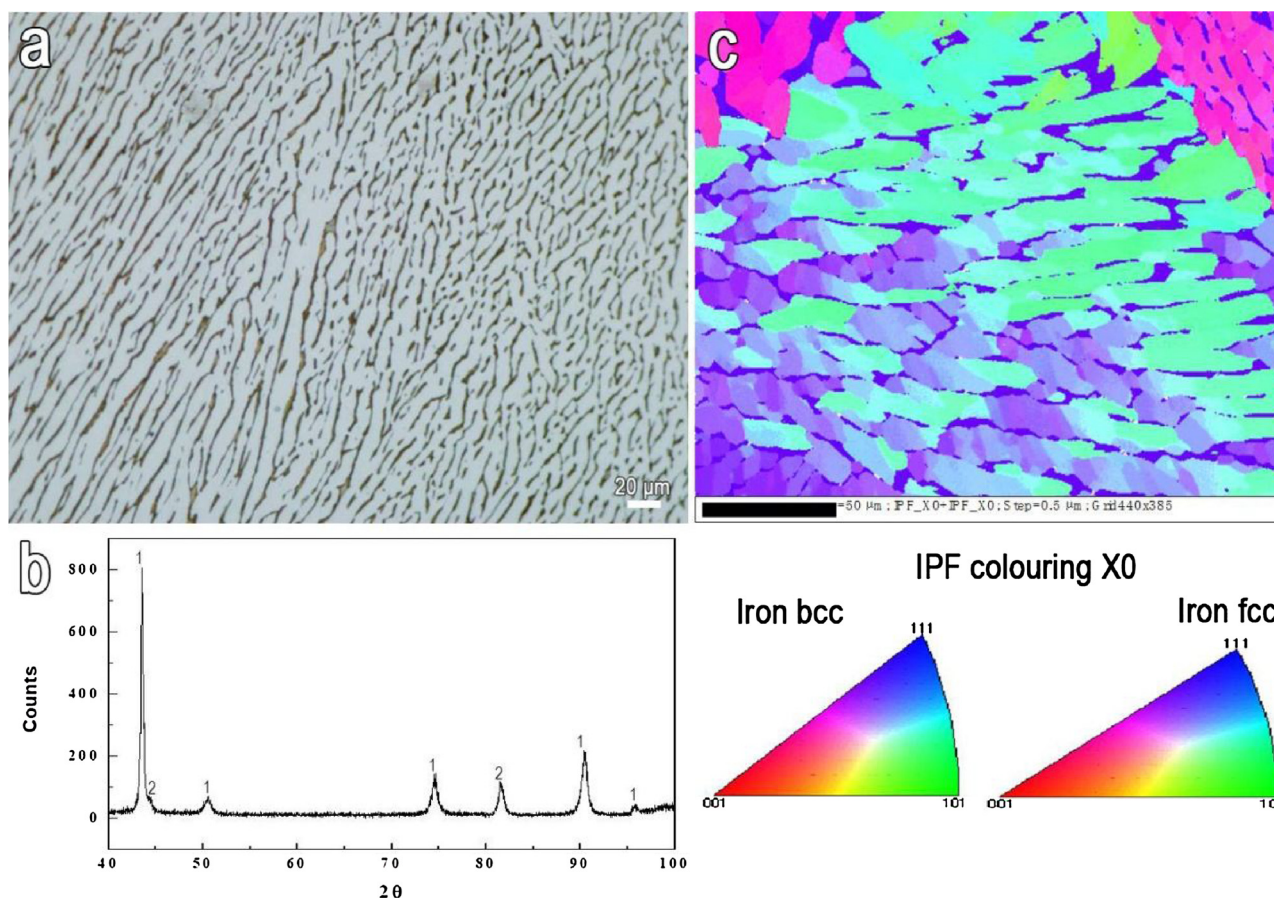


Fig. 1. Characterization of the $\text{FeCr}_{22}\text{Mo}_3\text{Ni}_{13}$ duplex alloy parallel to the growth direction. (a) Metallographic images showing ferritic phase (δ) with darker contrast dispersed in the austenite phase (γ) matrix with brighter contrast. (b) EBSD map showing the varied orientations in γ phase and almost identical orientations in δ phase. (c) XRD analysis showing that the duplex alloy is composed of the austenite (γ) and ferritic phases (δ). The peaks labeled by (1) correspond to γ phase and those labeled by (2) correspond to δ phase.

passive films.

Transmission electron microscopy (TEM) technique is of great advantages in resolving the issues correlated to the early-stage corrosion. We have employed this advanced TEM technique to investigate some issues of the pitting initiation as well as the passive film breakdown [16–26]. In our recent work, we successfully unraveled passive film evolution, from the metal surface to the metal/film interface, on austenitic alloys in chloride-containing media [25]. In the present work, using aberration-corrected transmission electron microscopy (Cs-corrected TEM) and a fast and precise super X-ray energy-dispersive spectrometer (Super-XEDS) analysis with four detectors, we simultaneously investigate the films on the ferrite and austenite phase and near the phase boundary, as well as the evolution of the passive film in chloride-containing media. This study provides some virtual experimental insights into the features of chloride ion attack on the passive film on duplex alloys.

2. Experimental

2.1. Duplex alloy preparation and characterization

The $\text{FeCr}_{22}\text{Mo}_3\text{Ni}_{13}$ duplex alloy was used as matrix on which the passive film was formed for the study. The thermal gradient directional solidification method was used to grow the duplex alloy.

2.2. Passive film formation

The duplex alloy rod was cut into cuboid-shaped test specimens of

dimensions $1.3 \times 2.2 \times 1.5$ mm, with one surface perpendicular to the axis direction (near [001] direction). The specimens were ground using silicon carbide papers and then polished electrochemically at -20 °C in HClO_4 (10 vol. %) + ethyl alcohol (90 vol. %) at 20–23 V, to remove the deformed layer and obtain the smooth surface. The specimens were subsequently sealed with thread sealing tape and olefin resin to be the electrodes for subsequent passivation treatments with (001) plane as future observing surface.

An AUTOLAB PGSTAT302N electrochemical workstation and a traditional three-electrode system were used in electrochemical experiments. The working electrode was the $\text{FeCr}_{22}\text{Mo}_3\text{Ni}_{13}$ duplex alloy, Pt was used as counter electrode and SCE (saturated with KCl) as reference electrode. Potentiodynamic polarization measurements were performed at a scan rate of 0.33 mV/s, in aerated $0.5 \text{ mol L}^{-1} \text{ H}_2\text{SO}_4$ and $0.5 \text{ mol L}^{-1} \text{ H}_2\text{SO}_4 + 0.25 \text{ mol L}^{-1} \text{ NaCl}$ electrolytes respectively.

2.3. TEM specimen preparation and technology

The cross-sectional TEM specimen was prepared by the conventional method. The passivated surfaces of two samples were bonded face-to-face, then thinned by grinding using variant grit silicon carbide papers up to 20 μm , polished with diamond paste, and finally thinned by ion-milling. The HAADF-STEM images were obtained by aberration-corrected transmission electron microscopy (Titan Cubed 60–300 kV microscope (FEI) fitted with a high-brightness field-emission gun (X-FEG), double Cs corrector from CEOS, and a monochromator operating at 300 kV).

In order to ensure formation of damage-free films during sample

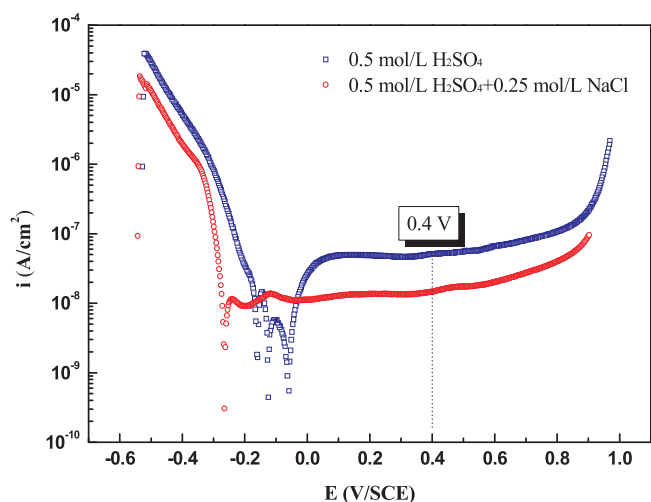


Fig. 2. Potentiodynamic polarization curve of FeCr₂₂Mo₃Ni₁₃ duplex alloy in 0.5 mol/L H₂SO₄ and 0.5 mol/L H₂SO₄ + 0.3 mol/L NaCl electrolytes.

preparation, the surfaces were not touched at all during sealing, passivating, rinsing and unsealing stages. Also, care was taken to avoid slipping during face-to-face bonding of the passivated surfaces. After the cross-sectional specimen was thinned by grinding, we directly performed the ion-milling without the dimpling step in order to further avoid mechanical damage.

3. Results and discussion

The microstructure characteristics of the duplex alloy as illustrated in Fig. 1 shows the presence of austenite and ferrite phases (Fig. 1a,b). Metallographic images of representative morphologies of the duplex alloy (Fig. 1a) shows the ferrite phase (δ) with darker contrast dispersed in the austenite phase (γ) matrix (with brighter contrast). Electron backscattered diffraction (EBSD) analysis indicates that the δ phase has an almost identical orientation, whereas the γ phase has varied orientations (Fig. 1c).

Potentiodynamic polarization measurements (Fig. 2) were performed firstly in aerated 0.5 mol/L H₂SO₄ and 0.5 mol/L H₂SO₄ + 0.25 mol/L NaCl electrolytes respectively, in order to determine a suitable passivation potential (400 mV / SCE was selected to be the passive film formation potential) in the passive region for the potentiostatic passivation process. The specimen was depolarized at -1.2 V/SCE for 30 s before potentiostatic passivation, in order to preclude formation of the native air-formed oxide layer. Then the potential was then stepped to 400 mV/SCE and maintained for 20 min at this potential to allow passive film formation.

Fig. 3a is the high angle annular dark field scanning transmission electron microscopic (HAADF-STEM) image of the passive film formed in 0.5 mol/L H₂SO₄ electrolyte. The passive film continuously covers the austenite (γ) and ferrite (δ) phase, but has a step-like unevenness at the γ/δ boundary region, with amplitude close to 7 nm between the

film/ δ and film/ γ interfaces. Careful analysis of the γ/δ boundary regions in a large number of passive films, showed the step-like unevenness to be prevalent, with the interface of film/ γ always lower than that of film/ δ . The uneven step might result from the electrochemical polishing or from variations in the growth rate of the films on the two phases. In order to clarify this, the air-formed oxide film was similarly investigated and the HAADF-STEM image shown in Fig. 3b reveals a very small step with amplitude of about 1.5 nm. The small step in the air-formed oxide implies that it does not originate from the electrochemical polishing pretreatment. Actually, the film growth process in an electrolyte involves transport of both dissolved metal ions from the matrix and oxygen in solution through the barrier layer, thus causing the metal/film interface to move towards the metal matrix side. The fact that the film/ γ interface is always lower than the film/ δ interface strongly implies that the passive film on the austenite has more pronounced ions transport rate and thus higher film growth rate than that on the ferrite phase. In tandem, the passive film on the austenite phase has a thicker equilibrium thickness (Fig. 3, about 4.5 nm to the austenite phase and 3.4 nm to the ferrite phase) since the equilibrium thickness is highly dependent on the diffusion of the reactive species in the oxide film [12].

It is noteworthy that, in chloride-free electrolyte (Fig. 3a), the film/matrix interface is well defined and straight, and the film has a homogeneous contrast in the HAADF imaging mode. In contrast, from the passive film formed in chloride-containing H₂SO₄ solution (Fig. 4) it is clear that the previously well-defined and straight interface in chloride-free solution has become indistinct. This is indisputably a consequence of chloride ion attack. Interestingly, the evolution of the films on the two phases is different. It is the outermost surface of the passive film on the ferrite phase that becomes undulating (labeled by the white arrows in Fig. 4b). On the other hand, the film/ γ interface becomes indistinct for the austenite phase (labeled by the purple arrows in Fig. 4c). This indicates that the chloride attack sites on the films differ for the austenite and ferrite phases.

By means of Super-X EDS mapping experiments (Fig. 5), we successfully obtained the evolution of the passive films, including the composition and the distribution of elemental Cl in the passive film. For the film formed in 0.5 mol/L H₂SO₄, Fig. 5a shows the element maps of Cr, O, Mo, Ni, and Fe. For the film formed in 0.5 mol/L H₂SO₄ + 0.3 mol/L NaCl electrolytes, Fig. 5b shows the chloride map together with Cr, O, Mo, Fe, and Ni. It is seen that chloride ions are incorporated into the passive films on both phases. Interestingly, Cl ions are mainly concentrated within the outer layer of the film on the ferrite phase, but penetrate the bulk of the film on the austenite phase. The findings from both the HAADF-STEM image and the Super-X EDS mapping show clearly that chloride ions attack the passive films on the two phases by different means, predominantly attacking the outer layer of the film on the ferrite phase, while attacking the interface of the film/ γ on the austenite phase. Evidently, the passive film on the austenite, with more pronounced ions transport rate deduced from the finding of the step-like unevenness at the γ/δ boundary region, is also favorable to the chloride transportation. Actually, migration and diffusion processes of chloride ions within passive films have been

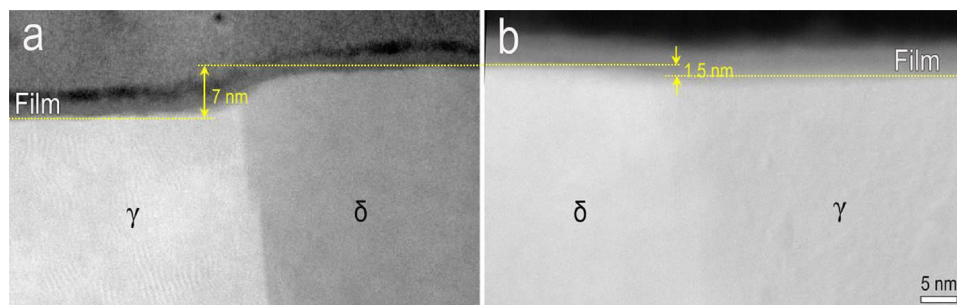


Fig. 3. Different growth rates of the passive films on the γ phase and δ phase. (a) HAADF-STEM image showing a passive film anodically formed in 0.5 mol/L H₂SO₄ electrolyte with step-like interface. The amplitude between the metal/film interfaces of the γ and δ phases is about 7 nm. (b) HAADF-STEM image showing a natural passive film formed in air, with remarkably reduced step amplitude.

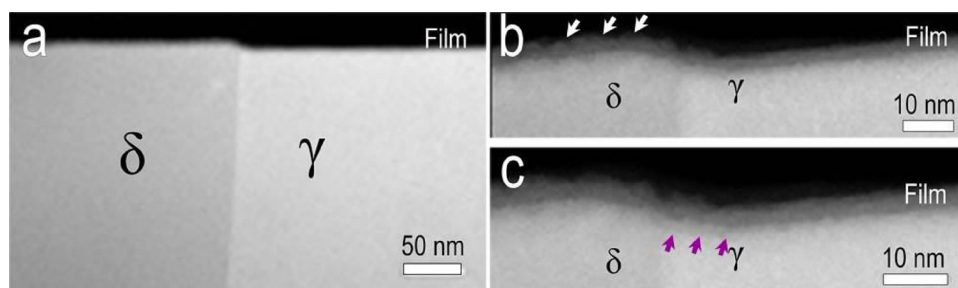


Fig. 4. Chloride attack on the passive film of $\text{FeCr}_{22}\text{Mo}_3\text{Ni}_{13}$ duplex alloy. (a) Low-magnification HAADF-STEM image showing the passive film anodically formed in 0.5 mol/L H_2SO_4 + 0.3 mol/L NaCl electrolytes. (b) Zoom-in image near the triple interface of $\delta/\gamma/\text{film}$ in (a) showing an undulating external film surface on the δ phase (labeled by white arrows), and a relatively smooth external surface on the γ phase. (c) Zoom-in image shows a larger view near the triple interface, wherein a blurred film/ γ interface comprising of some dots with

slightly darker contrast can be seen (labeled by purple arrows) (For interpretation of the references to colour in this figure legend, the reader is referred to the web version of this article).

considered to be closely correlated to the nature of passive film, such as compactness, defects (grain/phase boundary) [27–29], electronic properties (type/concentration of charge carriers) [30–32], etc. In our previous work on the austenite single crystal alloy, we directly observed atomic scale accumulation of chloride ions at the metal/film interface and the induced interfacial undulations [25], and proposed that the connected and traversed paths along the interface between nanocrystals and the amorphous zone in passive film provide ready paths for chloride ion transport. The strong implication is that full amorphization has greater tendency to resist localized attack due to the absence of the ready path (grain boundaries) for outward migration of cations or

inward migration of anions [29,33–35]. Cr is known as an ‘amorphization’ element, which could transform the passive film from well-defined spinel of iron to amorphous of Fe-Cr alloy when the Cr content was higher than 12% [12,33,36,37]. Furthermore, an increase in Cr content would increase the tendency to form glassy oxide films [35]. Element Cr is known to be partitioned to the ferrite phase of DSS. Accordingly, its passive film probably has more amorphous tendency, and the migration and diffusion of chloride ions within it would be more difficult than within that of the austenite.

Interestingly, although chloride ions are apt to penetrate the passive film on the austenite, a distinct concentration at the film/ γ interface, as

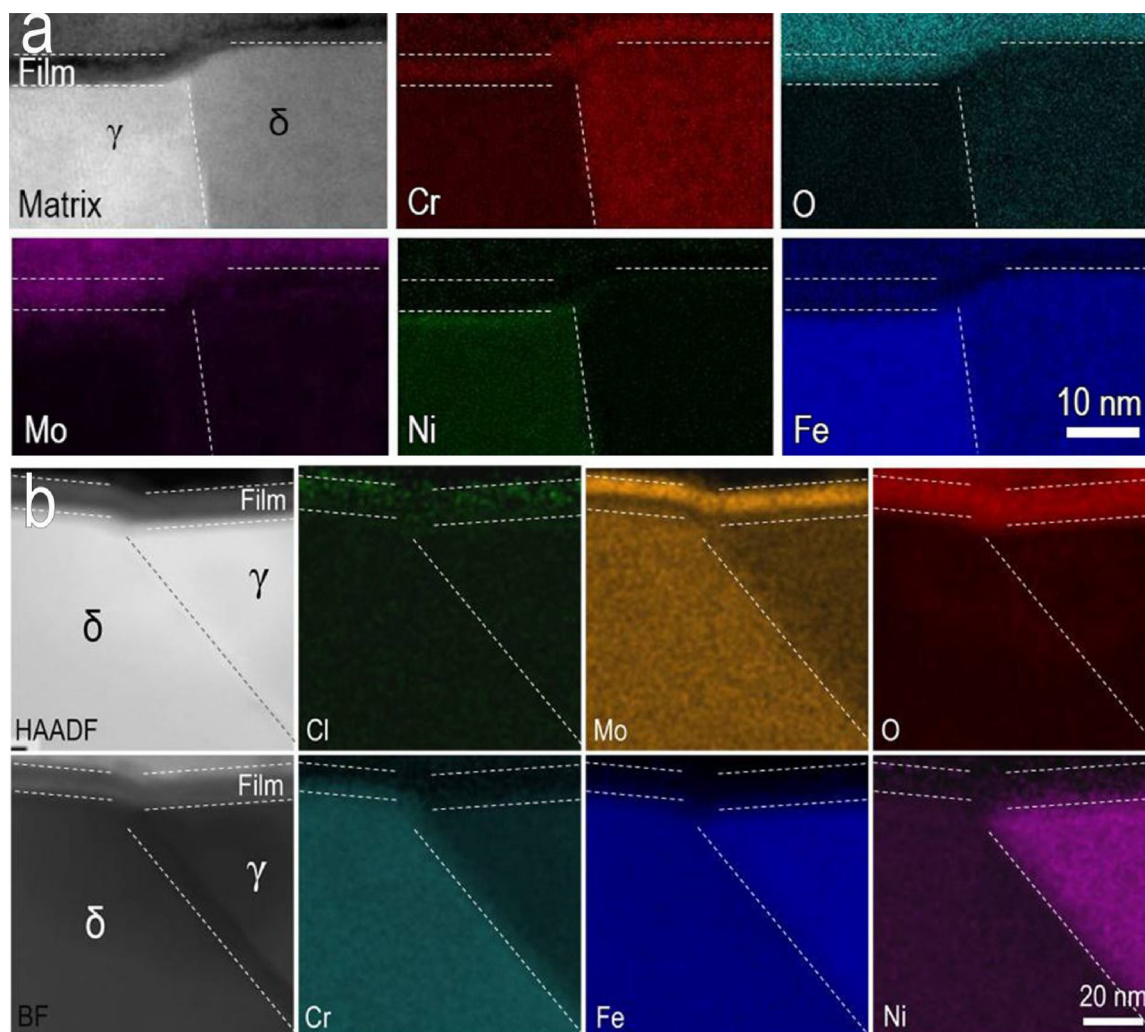


Fig. 5. Super-X EDS mapping showing chloride ions incorporated in the passive film and inducing composition evolution in the passive film. Element maps of the film formed in 0.5 mol/L H_2SO_4 (a) and 0.5 mol/L H_2SO_4 + 0.3 mol/L NaCl electrolytes (b) at 0.4 V/SCE for 30 min.

that of the FeCr₁₅Ni₁₅ single crystal in our previous work [25], did not occur here. This implies that, compared with the passive film anodically formed on the Mo-free Fe-Cr-Ni austenitic alloy, chloride ions transportation is greatly retarded within the passive film on the Mo-containing austenite phase of DSS. It has long been known that Mo is a typical element which improves the pitting corrosion resistance in steels [38–43]. Much of evidence and hypotheses on the ways through which Mo improve the resistance to chloride pitting can be mainly classified into two groups: one is Mo enrichment [39,41,44–46] and the other is Mo absent in the passive film [47–49]. In case of enrichment, Mo is considered to modify the composition and structure of the passive film to impede adsorption of Cl[−] onto the passive film surface as well as retard transportation of Cl[−] within the passive film, by thickening of the passive film [39,50], converting the ion selectivity of the passive film [40,45], eliminating the active surface sites [39,44,47,51], stabilizing Cr oxides [39], and enhancing the growth of a totally amorphous passive film [40,52]. In case of Mo absence in passive films, Mo is proposed to retard the corrosion process by the adsorption of MoO₄^{2−} [46,53,54].

According to Super-X EDS mapping (Fig. 5), the passive film, formed in the chloride-free electrolyte, is a Cr-rich oxide film (Cr map in Fig. 5a). Meanwhile, the Mo map features the strong noise signal implies that Mo is absent in the passive film. By contrast, in the chloride-containing electrolyte, the previous Cr-rich oxide film transforms to a thicker Mo-rich passive film (Mo map and Cr map in Fig. 5b). The film thickness ranged from 3.5 nm in H₂SO₄ electrolyte, and from 10–12 nm in H₂SO₄ + NaCl electrolyte. Mo is mainly enriched in the exterior region of the passive film. Actually, many previous studies showed that molybdenum tends to become enriched in the surface as Mo (IV) or/and Mo (VI) for the Mo-bearing stainless steels in acid chloride-containing media [40,46]. Meanwhile, the formation of Cr oxide is retarded to some extent [49]. The Mo(VI) oxide is usually claimed to have an improved stability [39,40] and thus is more resistant to chloride attack. Based on the EDS mapping results, it is strongly implied that the enrichment of Mo in the passive film is closely correlated to the interaction between chloride and Mo-containing matrix. Indeed, in almost all the previous studies where Mo was found to be enriched in the passive film, the used solution in which passive film was formed is chloride-containing. It is proposed that Cl[−] ions could extract Mo from the matrix into electrolyte by forming soluble MoCl_x complex. Then, the MoCl_x is further oxidized to be Mo oxide and enriched in the outer region of the passive film. In previous work [40,46], some researchers detected Mo³⁺ identical with MoCl₃ near the film/solution interface by XPS in the initially formed passive film. With an increase of the passivating time, Mo³⁺ was found to be disappeared, and Mo⁴⁺ and Mo⁶⁺ tend to appear in the outer region of the passive film. This also indicates that Cl[−] is prerequisite for Mo participation in the passive film. In other words, the defense function of element Mo would be activated only when the aggressive ions appears.

4. Conclusion

Using spherical aberration-corrected transmission electron microscopy, we have directly visualized the passive film on the γ/δ boundary region in duplex alloy as well as its evolution as induced by chloride from the out-of-plane direction. The passive film continuously covers the γ and δ phase but has a step-like unevenness at the γ/δ boundary. The passive film on the austenite has a more pronounced growth rate yielding the lower interface. Our experimental results suggest that the chloride ion attack mechanisms differ from austenite to ferrite phase, attacking the outmost surface of the passive film on ferrite (δ) phase and the interface of passive film/austenite phase. Based on the Super-X EDS analysis, aging in chloride-containing solution induces a thicker Mo-rich passive film from the original Cr-rich passive film.

Data availability

The raw/processed data required to reproduce these findings cannot be shared at this time due to legal or ethical reasons.

Acknowledgements

This work is supported by the National Natural Science Foundation of China (No. 51771212, 11327901, 51390473), the Key Research Program of Frontier Sciences CAS (QYZDJ-SSW-JSC010), the Innovation Fund in IMR (2017-ZD05). The authors are grateful to Prof. H. Wei for the help with the single crystal growth.

References

- [1] M. Femenia, J. Pan, C. Leygraf, Characterization of ferrite-austenite boundary region of duplex stainless steels by SAES, *J. Electrochem. Soc.* 151 (2004) B581–B585.
- [2] J.O. Nilsson, Super duplex stainless-steels, *Mater. Sci. Technol.* 8 (1992) 685–700.
- [3] C.O.A. Olsson, The influence of nitrogen and molybdenum on passive films formed on the austenoferritic stainless-steel-2205 studied by AES and XPS, *Corros. Sci.* 37 (1995) 467–479.
- [4] L.F. GarfiasMesias, J.M. Sykes, C.D.S. Tuck, The effect of phase compositions on the pitting corrosion of 25 cr duplex stainless steel in chloride solutions, *Corros. Sci.* 38 (1996) 1319–1330.
- [5] L. Weber, P.J. Uggowitzer, Partitioning of chromium and molybdenum in super duplex stainless steels with respect to nitrogen and nickel content, *Mater. Sci. Eng. A* 242 (1998) 222–229.
- [6] E. Schmidt-Rieder, M. Ashworth, J.P.G. Farr, The effect of nitrogen on the stability of the passive film on a zeron 100 super duplex stainless steel, *Electrochim. Solid-State Lett.* 2 (1999) 19–21.
- [7] V. Vignat, O. Delrue, O. Heintz, J. Peultier, Influence of the passive film properties and residual stresses on the micro-electrochemical behavior of duplex stainless steels, *Electrochim. Acta* 55 (2010) 7118–7125.
- [8] V. Vignat, H. Zhang, O. Delrue, O. Heintz, I. Popa, J. Peultier, Influence of long-term ageing in solution containing chloride ions on the passivity and the corrosion resistance of duplex stainless steels, *Corros. Sci.* 53 (2011) 894–903.
- [9] H. He, T. Zhang, C.Z. Zhao, K. Hou, G.Z. Meng, Y.W. Shao, F.H. Wang, Effect of alternating voltage passivation on the corrosion resistance of duplex stainless steel, *J. Appl. Electrochem.* 39 (2009) 737–745.
- [10] W. Fredriksson, K. Edstrom, C.O. Olsson, XPS analysis of manganese in stainless steel passive films on 1.4432 and the lean duplex 1.4162, *Corros. Sci.* 52 (2010) 2505–2510.
- [11] C. Donik, D. Mandrino, M. Jenko, Depth profiling and angular dependent XPS analysis of ultra thin oxide film on duplex stainless steel, *Vacuum* 84 (2010) 1266–1269.
- [12] M.P. Ryan, R.C. Newman, G.E. Thompson, A scanning-tunneling-microscopy study of structure and structural relaxation in passive oxide-films on Fe-Cr alloys, *Philos. Mag. B* 70 (1994) 241–251.
- [13] L. Garfias, D. Siconolfi, In situ high-resolution microscopy on duplex stainless steels, *J. Electrochem. Soc.* 147 (2000) 2525–2531.
- [14] Y. Jiang, H. Tan, Z. Wang, J. Hong, L. Jiang, J. Li, Influence of Creq/Nieq on pitting corrosion resistance and mechanical properties of UNS S32304 duplex stainless steel welded joints, *Corros. Sci.* 70 (2013) 252–259.
- [15] L.Q. Guo, M.C. Lin, L.J. Qiao, A.A. Volinsky, Duplex stainless steel passive film electrical properties studied by in situ current sensing atomic force microscopy, *Corros. Sci.* 78 (2014) 55–62.
- [16] S.J. Zheng, Y.J. Wang, B. Zhang, Y.L. Zhu, C. Liu, P. Hu, X.L. Ma, Identification of MnCr₂O₄ nano-octahedron in catalysing pitting corrosion of austenitic stainless steels, *Acta Mater.* 58 (2010) 5070–5085.
- [17] Y.T. Zhou, Y.B. Xue, D. Chen, Y.J. Wang, B. Zhang, X.L. Ma, Atomic-scale configurations of synchroshear-induced deformation twins in the ionic MnS crystal, *Sci. Rep.* 4 (2014) 5118.
- [18] Y.T. Zhou, B. Zhang, S.J. Zheng, J. Wang, X.Y. San, X.L. Ma, Atomic-scale decoration for improving the pitting corrosion resistance of austenitic stainless steels, *Sci. Rep.* 4 (2014) 3604.
- [19] J. Wang, B. Zhang, Y.T. Zhou, X.L. Ma, Multiple twins of a decagonal approximant embedded in S-Al₂CuMg phase resulting in pitting initiation of a 2024Al alloy, *Acta Mater.* 82 (2015) 22–31.
- [20] B. Zhang, J. Wang, B. Wu, Y.T. Zhou, X.L. Ma, Quasi-in-situ ex-polarized TEM observation on dissolution of MnS inclusions and metastable pitting of austenitic stainless steel, *Corros. Sci.* 100 (2015) 295–305.
- [21] Y.T. Zhou, Y.J. Wang, S.J. Zheng, B. Zhang, X.L. Ma, Strain-induced preferential dissolution at the dislocation emergences in MnS: An atomic scale study, *Philos. Mag.* 95 (2015) 2365–2375.
- [22] J. Wang, B. Zhang, B. Wu, X.L. Ma, Size-dependent role of s phase in pitting initiation of 2024Al alloy, *Corros. Sci.* 105 (2016) 183–189.
- [23] B. Zhang, J. Wang, B. Wu, E.E. Oguzie, K. Luo, X.L. Ma, Direct observation of atomic-scale origins of local dissolution in Al-Cu-Mg alloys, *Sci. Rep.* 6 (2016) 39525.
- [24] X.Y. San, B. Zhang, B. Wu, X.X. Wei, E.E. Oguzie, X.L. Ma, Investigating the effect of

- Cu-rich phase on the corrosion behavior of Super 304H austenitic stainless steel by TEM, *Corros. Sci.* 130 (2018) 143–152.
- [25] B. Zhang, J. Wang, B. Wu, X.W. Guo, Y.J. Wang, D. Chen, Y.C. Zhang, K. Du, E.E. Oguzie, X.L. Ma, Unmasking chloride attack on the passive film of metals, *Nat. Commun.* 9 (2018) 2559.
- [26] B. Zhang, X.Y. San, X.X. Wei, B. Wu, S.J. Zheng, Y.T. Zhou, X.H. Shao, Q.Q. Jin, L.X. Yang, E.E. Oguzie, X.L. Ma, Quasi-in-situ observing the growth of native oxide film on the FeCr₁₅Ni₁₅ austenitic alloy by TEM, *Corros. Sci.* 140 (2018) 1–7.
- [27] S.C. Hendy, N.J. Laycock, M.P. Ryan, Atomistic modeling of cation transport in the passive film on iron and implications for models of growth kinetics, *J. Electrochem. Soc.* 152 (2005) B271–B276.
- [28] P. Marcus, V. Maurice, H.H. Strehblow, Localized corrosion (pitting): a model of passivity breakdown including the role of the oxide layer nanostructure, *Corros. Sci.* 50 (2008) 2698–2704.
- [29] G. Okamoto, Passive film of 18-8 stainless-steel structure and its function, *Corros. Sci.* 13 (1973) 471–489.
- [30] B. Ter-Ovanesian, C. Alemany-Dumont, B. Normand, Electronic and transport properties of passive films grown on different Ni-Cr binary alloys in relation to the pitting susceptibility, *Electrochim. Acta* 133 (2014) 373–381.
- [31] E. McCafferty, Relationship between the isoelectric point (pHpzc) and the potential of zero charge (E_{pzc}) for passive metals, *Electrochim. Acta* 55 (2010) 1630–1637.
- [32] L.F. Lin, C.Y. Chao, D.D. Macdonald, A point-defect model for anodic passive films. 2. Chemical breakdown and pit initiation, *J. Electrochem. Soc.* 128 (1981) 1194–1198.
- [33] V. Maurice, W.P. Yang, P. Marcus, XPS and STM investigation of the passive film formed on Cr(110) single-crystal surfaces, *J. Electrochem. Soc.* 141 (1994) 3016–3027.
- [34] J.S.L. Leach, The role of surface films in corrosion and oxidation, *Surf. Sci.* 53 (1975) 257–271.
- [35] U. Bertocci, J. Kruger, Studies of passive film breakdown by detection and analysis of electrochemical noise, *Surf. Sci.* 101 (1980) 608–618.
- [36] M.P. Ryan, R.C. Newman, G.E. Thompson, Atomically resolved STM of oxide film structures on Fe-Cr alloys during passivation in sulfuric-acid-solution, *J. Electrochem. Soc.* 141 (1994) L164–L165.
- [37] V. Maurice, W.P. Yang, P. Marcus, XPS and STM study of passive films formed on Fe-22Cr(110) single-crystal surfaces, *J. Electrochem. Soc.* 143 (1996) 1182–1200.
- [38] K.H. Lo, C.H. Shek, J.K.L. Lai, Recent developments in stainless steels, *Mater. Sci. Eng. R Rep.* 65 (2009) 39–104.
- [39] K. Sugimoto, Y. Sawada, Role of molybdenum additions to austenitic stainless-steels in inhibition of pitting in acid chloride solutions, *Corros. Sci.* 17 (1977) 425–445.
- [40] C.R. Clayton, Y.C. Lu, A bipolar model of the passivity of stainless-steel-the role of Mo addition, *J. Electrochem. Soc.* 133 (1986) 2465–2473.
- [41] M.F. Montemor, A.M.P. Simoes, M.G.S. Ferreira, M.D. Belo, The role of Mo in the chemical composition and semiconductive behaviour of oxide films formed on stainless steels, *Corros. Sci.* 41 (1999) 17–34.
- [42] R. Kirchheim, B. Heine, H. Fischmeister, S. Hofmann, H. Knote, U. Stolz, The passivity of iron-chromium alloys, *Corros. Sci.* 29 (1989) 899–917.
- [43] K. Asami, K. Hashimoto, S. Shimodaira, XPS study of passivity of a series of iron-chromium alloys in sulfuric-acid, *Corros. Sci.* 18 (1978) 151–160.
- [44] C. Leygraf, G. Hultquist, I. Olefjord, B.O. Elfstrom, V.M. Knyazheva, A.V. Plaskeyev, Y.M. Kolotyrlin, Selective dissolution and surface enrichment of alloy components of passivated Fe₁₈Cr and Fe₁₈Cr₃Mo single-crystals, *Corros. Sci.* 19 (1979) 343–357.
- [45] K. Asami, M. Naka, K. Hashimoto, T. Masumoto, Effect of molybdenum on the anodic behavior of amorphous Fe-Cr-Mo-B alloys in hydrochloric-acid, *J. Electrochem. Soc.* 127 (1980) 2130–2138.
- [46] C.R. Clayton, Y.C. Lu, A bipolar model of the passivity of stainless-steels. 3. The mechanism of MoO₄²⁻ formation and incorporation, *Corros. Sci.* 29 (1989) 881–898.
- [47] I. Olefjord, B.O. Elfstrom, The composition of the surface during passivation of stainless-steels, *Corrosion* 38 (1982) 46–52.
- [48] H. Habazaki, A. Kawashima, K. Asami, K. Hashimoto, The corrosion behavior of amorphous Fe-Cr-Mo-P-C and Fe-Cr-W-P-C alloys in 6-M HCl solution, *Corros. Sci.* 33 (1992) 225–236.
- [49] M.W. Tan, E. Akiyama, A. Kawashima, K. Asami, K. Hashimoto, The effect of air exposure on the corrosion behavior of amorphous Fe-8Cr-Mo-13P-7C alloys in 1 M HCl, *Corros. Sci.* 37 (1995) 1289–1301.
- [50] J. Moon, H.Y. Ha, S.J. Park, T.H. Lee, J.H. Jang, C.H. Lee, H.N. Han, H.U. Hong, Effect of Mo and Cr additions on the microstructure, mechanical properties and pitting corrosion resistance of austenitic Fe-30Mn-10.5Al-1.1C lightweight steels, *J. Alloys. Compd.* 775 (2019) 1136–1146.
- [51] K. Hashimoto, K. Asami, K. Teramoto, X-ray photoelectron spectroscopic study on the role of molybdenum in increasing the corrosion-resistance of ferritic stainless-steels in HCl, *Corros. Sci.* 19 (1979) 3–14.
- [52] T.P. Hoar, On corrosion-resistant materials, *J. Electrochem. Soc.* 117 (1970) C17.
- [53] K. Sugimoto, Y. Sawada, Role of alloyed molybdenum in austenitic stainless-steels in inhibition of pitting in neutral halide solutions, *Corrosion* 32 (1976) 347–352.
- [54] H. Ogawa, H. Omata, I. Itoh, H. Okada, Auger-electron spectroscopic and electrochemical analysis of effect of alloying elements on passivation behavior of stainless-steels, *Corrosion* 34 (1978) 52–60.